

## 7th International Conference on Crack Paths

## Crack field analysis by optical DIC of short cracks in Zircaloy-4

Xiao Su<sup>a,\*</sup>, Weifeng Wan<sup>b</sup>, Fionn P.E. Dunne<sup>b</sup>, T. James Marrow<sup>a</sup><sup>a</sup>Department of Materials, University of Oxford, Parks Road, Oxford OX1 3PH, UK<sup>b</sup>Department of Materials, Royal School of Mines, Imperial College London, London SW7 2AZ, UK

---

**Abstract**

The prediction of fatigue life is most difficult for short cracks, as their local conditions may differ from what is predicted using the remote applied loading and crack geometry. Digital image correlation (DIC) can be utilized to analyze images from an optical microscope (OM), which facilitates the local characterization of the crack field. This paper presents a Finite-Element-based approach that uses DIC-obtained displacement data to retrieve the crack field and quantify the local crack driving force. With the assumption of linear anisotropic elasticity, the change in both the Mode I and Mode II crack intensity factors over a fatigue cycle can be extracted using the interaction integral method. This allows the determination of the local driving force for short crack propagation. The application of this method is demonstrated by the full-field analysis of short fatigue cracks in blocky alpha Zircaloy-4. The sensitivity of the analysis is investigated to factors that include DIC subset size, uncertainties in crack tip position and lower quality data in the crack vicinity. This technique requires no prior knowledge of theoretical solutions or far-field boundary conditions, and it can be applied to the tip of a tortuous crack by defining an appropriate local frame of reference. The analysis is applied here to cracks under similar mode I loading that propagate on the prism plane at different rates in directions that are parallel and perpendicular to the c-axis of the hexagonal unit cell.

© 2021 The Authors. Published by Elsevier B.V.

This is an open access article under the CC BY-NC-ND license (<https://creativecommons.org/licenses/by-nc-nd/4.0>)

Peer-review under responsibility of CP 2021 – Guest Editors

**Keywords:** Stress intensity factor; Digital image correlation; Short crack; Crack field; Finite element analysis

---

**1. Introduction**

In order to ensure the safety and reliability of structural materials, emphasis has been put on the investigation of crack propagation mechanisms. The well-known Paris law uses the stress intensity factor range,  $\Delta K$ , as a single-

\* Corresponding author.

E-mail address: [xiao.su@materials.ox.ac.uk](mailto:xiao.su@materials.ox.ac.uk)

parameter characterization of crack tip conditions that allows a crack to propagate. In practical cases, the fatigue lifetime in short crack regime constitutes a major part of components' full life, but its prediction from remote loading conditions is often inaccurate as the observed rates of growth can vary greatly with crack length. This results from the microstructural sensitivity of short cracks, where the crack tip grows within a changing environment of local stresses and barriers to crack propagation [King et al. (2011); Marrow et al. (2014)]. To improve the reliability of life prediction models for short cracks [Wilkinson (2001); Christ, Fritzen, and Köster (2014)], experimental investigations of crack tip fields are necessary.

Full-field techniques with sufficient spatial resolution provide good options to measure the actual fields directly at the crack tip region. Digital Image Correlation, first introduced by Peter and Ranson [Peters and Ranson (1982)], is a common and powerful approach to measure the full-field displacement on a specimen surface. It is achieved by the cross-correlation of recorded digital images, as its name suggests. Precise measurement of displacement relies on accurate tracking of subset patterns between the reference and deformed images. With various algorithms such as the Iterative spatial domain cross-correlation algorithm [Bruck et al. (1989); Vend Roux and Knauss (1998)] and the peak-finding algorithm [Hung and Voloshin (2003); Chen et al. (1993)], sub-pixel accuracy can be achieved in displacement registration, which facilitates the observation of short cracks in high resolution images [Duff and Marrow (2013)].

To analyze the field information obtained by measurements, it was common in the literature to retrieve the crack field using a field fitting approach [Newman and Raju (1986); Limodin et al. (2009); J. Réthoré et al. (2011)]. Theoretical solutions, such as the Williams field solution, are necessary in determining the field control parameters in field fitting approaches. For crack tip fields, work done by Liu and Lyons employed McNeill's method [McNeill, Peters, and Sutton (1987)] to calculate the stress intensity factors for Inconel 718 [Liu et al. (1998)]. For mixed mode loading, stress intensity factors were estimated by extended field fitting of image correlation results [Roux and Hild (2006)]. The field fitting approach has also been applied to three-dimensional digital volume correlation analysis [Julien Réthoré et al. (2012)]. One drawback of this technique lies in the sensitivity to accurate definition of the crack tip location [McNeill, Peters, and Sutton (1987)].

An alternative way to deal with the DIC data is the direct evaluation of the J-integral. The JMAN method, proposed by Becker et al. [Becker et al. (2012); Becker, Marrow, and Tait (2011)], demonstrated the potential of using a domain integral in post-processing the measurement data. Other feasible integrals have also been reported in the literature, such as [Moutou Pitti, Badulescu, and Grédiac (2014)]. The path independence of this approach provides the advantage of evaluating the field control parameters with a path selection that is less sensitive to crack tip uncertainty, and the use of finite element analysis can allow non-linear behaviour to be addressed also.

Standard finite element software packages can be employed to perform the aforementioned integral evaluations. Barhli et al. [Barhli et al. (2017)] presented a novel method to extract the stress intensity factors with combined use of DIC and finite element simulations, where the virtual crack extension method was applied. Koko et al. verified the accuracy of this method, and a related and novel method to analyse stress intensity factors from diffraction-measured strain fields, in a study of a long fatigue crack in a compact tension specimen [Koko et al. (2020)]. In this study, we will extend this method to investigate the displacement fields of short fatigue cracks, propagating on crystallographic planes in a polycrystalline zirconium alloy. To avoid the interference of the low-quality data points around the crack face, a 'forbidden' zone is applied to exclude these inputs. The effects of subset size, crack tip uncertainty and forbidden zone size are also discussed in this paper.

## 2. Material and methods

The full description of the experiment that provided the raw data has been published elsewhere [Xu, Wan, and Dunne (2021)]; the relevant details are summarized here briefly. The material was from a pair of edge-notched Zircaloy-4 beam samples (Sample A and B), where the edge notch was introduced by Electrical Discharge Machining (EDM). As-received Zircaloy-4 plates (average grain size approximately 13.5  $\mu\text{m}$ ) were heat treated at 800°C for 2 weeks to generate 'blocky alpha' grains of size order 400  $\mu\text{m}$ . Their polycrystal microstructures are shown in Fig. 1. Sprayed with silica speckles of 1  $\mu\text{m}$ , they were loaded cyclically in three-point bend testing with a maximum load of 800N and *R*-ratio of 0. The details of sample geometry, notch shape and distance between the two fixed supporting pins are given in Table. 1. The samples were observed in situ with an optical Questar Microscope Lens (QM-100).

Images were recorded by CCD camera and the working distance was set of about 150mm. The pixel resolution of the optical microscope was 1 $\mu$ m.

Table 1. Geometry, edge-notch shape and distance between supporting pins (separated by 10 mm).

Sample	Geometry (mm)	Notch Shape ( $\mu$ m)
A	Height 3.18, Thickness 3.02, Length 12.01	Notch Height 270, Notch Width 150
B	Height 3.17, Thickness 2.93, Length 12	Notch Height 300, Notch Width 150

The DIC analyses in this work were performed between successive images of the unloaded and peak-loaded conditions during a single monotonic fatigue cycle, as shown in Fig. 1(b), using standard digital image correlation software (LaVision DaVis 8.4.0). The legacy mode Fast Fourier Transform correlation was used with the multi-pass option, where the default final subset size was set to 96 $\times$ 96 pixels with an overlap of 75%. A median filter [Westerweel and Scarano (2005)] was applied during vector post-processing to detect and remove bad results. A vector will be removed if the residual is larger than 2 times the standard deviation of its neighbours. Empty spaces were filled up by interpolated vectors which need at least two neighbour vectors. The fill-up was an iterative process, where interpolated vectors of the previous step was employed in subsequent iterations. This paper presents data obtained for cracks observed at 2400 cycles (Sample A) and 2200 cycles (Sample B), where the crack lengths are 230 $\mu$ m and 252 $\mu$ m respectively.

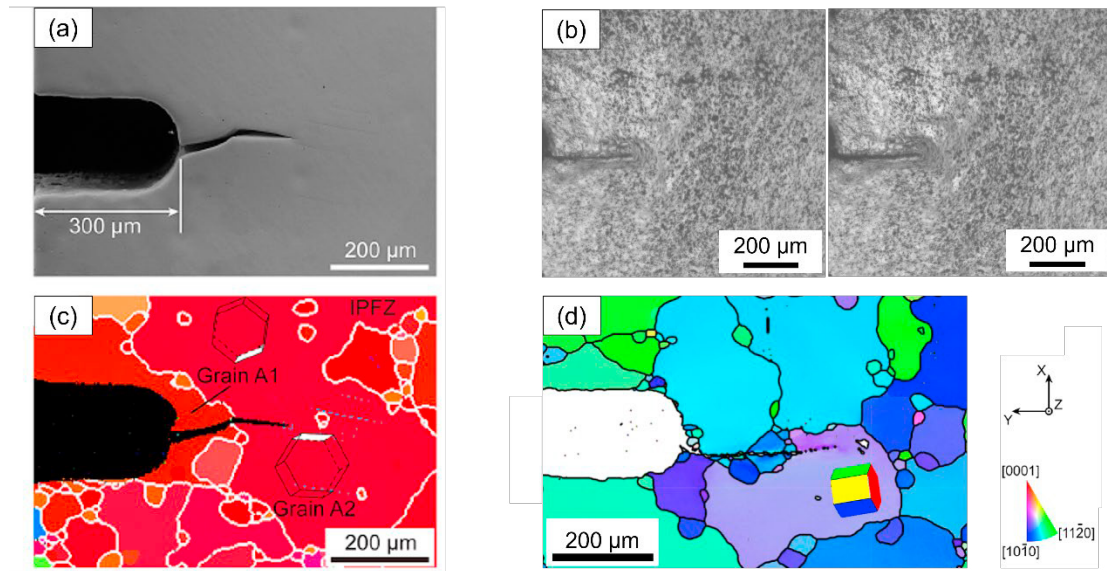


Fig. 1. (a) SEM image of sample A; (b) Optical images of sample B (unloaded and peak-loaded); (c) Inverse pole figure of the z-axis: sample A; (d) Inverse pole figure of the z-axis: sample B.

The post-processing procedure is illustrated in Fig. 2. In this method, the finite element model is registered to the DIC-obtained displacement field. The same grid is established in the finite element model, with each node corresponding to a displacement data point. The crack tip position is assessed, and a horizontal crack is inserted in the mesh. To accommodate the crack, the region in the vicinity of the crack is re-meshed. The data points obtained by DIC are injected as local boundary conditions, point by point. After defining the material properties in the model (i.e., assumption of linear anisotropic elasticity) a finite element analysis using CPS4 elements is performed to obtain the stress and strain fields. Within the region of data in the crack vicinity that is excluded during the finite element registration (i.e., within the ‘forbidden zone’), the nodal displacements are obtained by static equilibrium. Finally the J-integral can be calculated using the inbuilt algorithms (virtual crack extension) in the finite element software ABAQUS (version 6.14). The change in both the Mode I and Mode II crack intensity factors range,  $\Delta K_I$  and  $\Delta K_{II}$ , over

a fatigue cycle can then be extracted using the interaction integral method [Shih and Asaro (1989)], also implemented in ABAQUS.

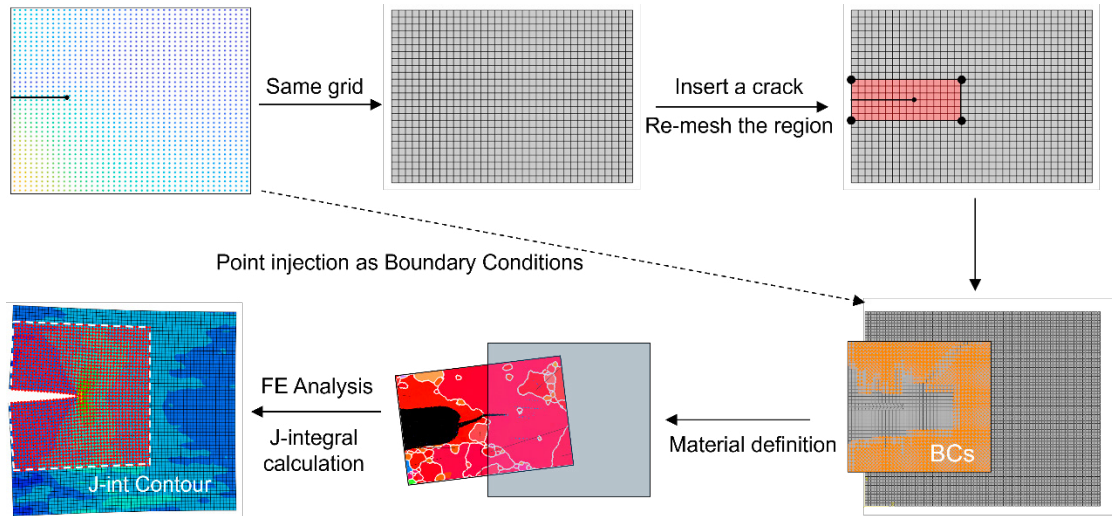


Fig. 2. Steps of the Finite Element post-processing of DIC-obtained displacement field.

For sample A, the crack is kinked in the imaged area, and it would be inclined to the reference axes if DIC and post-processing were performed with the original images. The objective is to quantify the J-integral and stress intensity factors for continued propagation in the direction of the crack, so the images were cropped and rotated beforehand to just retain a single horizontal crack segment in the region of interest, as shown in Fig. 3(a). These facilities the modeling process in finite element analysis. Fig. 3(b) presents a typical displacement field obtained by DIC after this processing.

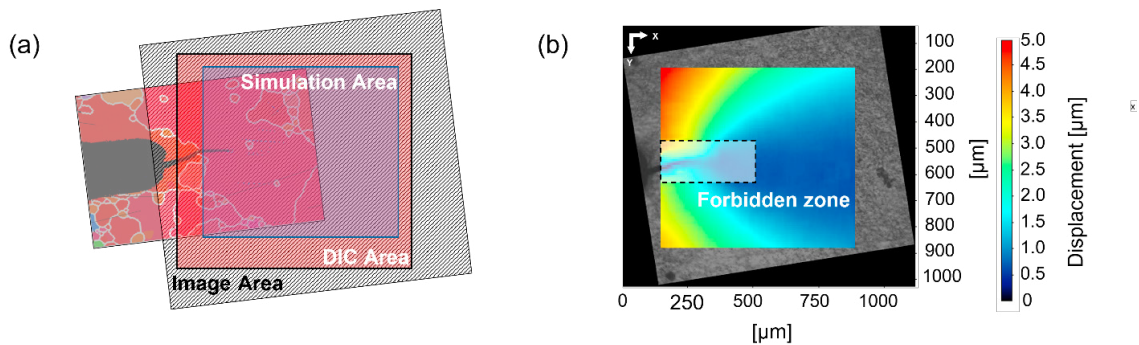


Fig. 3. Rotation of the original image and selection of the field data: (a) relative positions; (b) forbidden zone.

An inherent issue of digital image correlation involves the data points in the crack vicinity. It is well known that digital image correlation can fail to determine the displacement vectors satisfactorily near to a discontinuity [McNeill, Peters, and Sutton (1987)], which means that results can be erroneous in the vicinity of crack faces and sample edges. To solve that, the forbidden zone is used to exclude the crack region during the injection of boundary conditions, as shown in Fig.3(b). The minimum size forbidden zone should contain all the low-quality data where the correlation coefficient is low (i.e., the normalized correlation value is less than 0.95), approximately corresponding to a  $160 \times 75$  pixels area in this work for the two series of images. The default size of forbidden zone was set to  $200 \times 100$  pixels.

### 3. Results and discussions

With the assumption of pure mode I loading, which is the intended loading for a straight crack in the edge-notched bend specimen, the theoretical estimates of stress intensity factor range for these two samples using equation (1) from [Anderson (2017)] are  $15.36 \pm 0.24 \text{ MPa} \cdot \text{m}^{0.5}$  and  $16.85 \pm 0.27 \text{ MPa} \cdot \text{m}^{0.5}$  respectively, considering the uncertainty from errors in the precision of load  $\pm 0.5\%$ , errors in the precision of specimen dimensions measurement  $\pm 20 \mu\text{m}$  and errors in the measurement of crack length  $\pm 5 \mu\text{m}$ . In the equation  $P$  is the load applied on the three-point beam,  $S$  the distance between the supporting pins,  $W$  and  $B$  the height and thickness of the beam, and  $a_e$  is the effective crack length. The mode I stress intensity factor ranges obtained by this work (Table. 2), which do not use any information on the load and specimen geometry, are close to these values, as expected.

$$\Delta K = \frac{P}{B\sqrt{W}} f\left(\frac{a_e}{W}\right)$$

$$f\left(\frac{a_e}{W}\right) = \frac{3\left(\frac{S}{W}\right)\sqrt{\frac{a_e}{W}}}{2\left(1+2\left(\frac{a_e}{W}\right)\right)\left(1-\frac{a_e}{W}\right)^{3/2}} \left\{1.99 - \frac{a_e}{W}\left(1 - \frac{a_e}{W}\right)[2.15 - 3.93\left(\frac{a_e}{W}\right) + 2.7\left(\frac{a_e}{W}\right)^2]\right\} \quad (1)$$

Table 2. Mode I and mode II stress intensity factors for sample A and B, obtained by this work using subset size  $96 \times 96$  pixels, overlap of 75% with forbidden zone size  $200 \times 100$  pixels

Sample	Mode I stress intensity factor range, $\Delta K_I, \text{MPa} \cdot \text{m}^{0.5}$	Mode II stress intensity factor range, $\Delta K_{II}, \text{MPa} \cdot \text{m}^{0.5}$
A	$16.98 \pm 0.42$	$0.37 \pm 0.21$
B	$15.95 \pm 0.48$	$0.65 \pm 0.64$

The local analysis also detects a small degree of mode II loading. The ability to extract of both mode I and mode II stress intensity factors, especially mode II, creates a new opportunity to characterize mixed mode loading in the local crack frame with full-field measurements. The local displacement field is the driving factor of crack propagation, and the proposed method is able to obtain information of the relevant field-control parameters. Future studies may examine crack growth with more significant kinking of the crack tip to better understand the effect this has on the local crack growth rate.

The two studied cracks grew under similar mode I loading (dominating) but they showed quite different growth rates in the experiments:  $0.15 \mu\text{m}/\text{cycle}$  for sample A and  $0.35 \mu\text{m}/\text{cycle}$  for sample B. Fig.1(c) and (d) show that the crack in sample A propagated on the prism plane and perpendicular to the c-axis, while the crack in sample B propagated on the same prism plane but along the c-axis. Detailed discussion related to the rate behaviour with crystallographic direction can be found in [Wan and Dunne (2020)].

For digital image correlation, there is a compromise between spatial resolution and data uncertainty. If large subset size is used, the uncertainty is minimized during the image correlation process, simply because that large subset contains more information for such operation [Bornert et al. (2009)]. On the other hand, details might be lost as a result of sparse field data. For the J-integral calculation, careful consideration is also needed with regard to the crack tip region. Previous research has found some sensitivity to the crack tip position and the difficulty of dealing with the low-quality data near discontinuities [S. Roux, Réthoré, and Hild (2009); Stéphane Roux and Hild (2006)]. Therefore, the sensitivity of the  $\Delta K$  values to the DIC subset size, error in crack tip position and forbidden zone size were considered further.

To investigate the effect of subset size during digital image correlation, four different square subset sizes were considered from  $48 \times 48$  pixels to  $128 \times 128$  pixels, all with 75% overlap. Fig. 4 illustrates the results, where each point represents the average value for the full range of integral contours (13–42 contours, depending on subset size), and the error bar shows the standard deviation of the  $\Delta K$  values over these contours. There is a general trend for increasing error as the physical size of the subset decreases, which is due to the decreasing number of features available within

each subset to track the displacement field in the correlation analysis, which influences the boundary conditions in the J-integral calculation. For sample B, the results are similar with smaller uncertainty in the result at larger subset size.

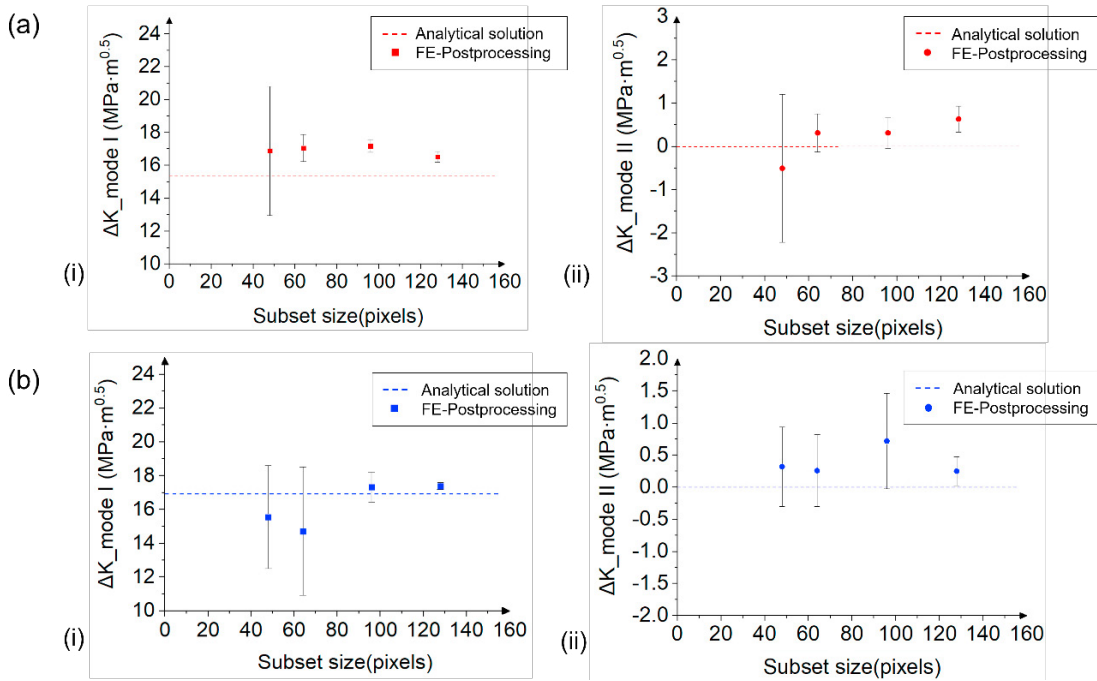


Fig. 4. Effect of DIC subset size on the calculation of stress intensity factors. (red: sample A; blue: sample B; rectangular: mode I; circle: mode II). The horizontal line shows the expected value for pure bending of the specimen.

Fig. 5(a) exhibits the effect when crack position uncertainties are introduced in the input data. Subset size  $96 \times 96$  pixels was used for DIC, with an overlap of 75%. The expected uncertainty in the crack tip position from the optical observations is less than  $5 \mu\text{m}$ , and although the crack length was changed up to  $\pm 30 \mu\text{m}$  from its known position in the different cases, there were only a minor effect on the range of stress intensity factor. In the worst case with crack tip position error up to  $30 \mu\text{m}$ , or an error in  $a/W$  of approximately 1%, the mean error in mode I stress intensity factor range,  $\Delta K_I$ , is less than 5%.

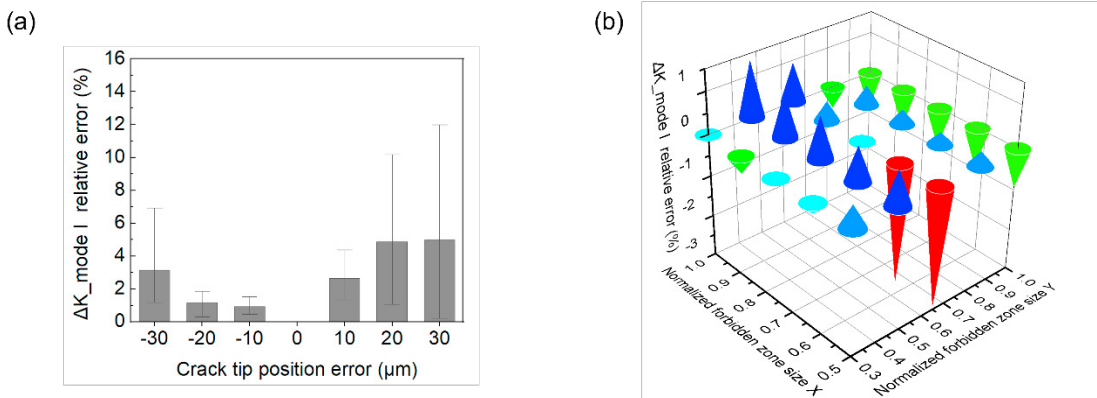


Fig. 5. (a) Effect of erroneous crack tip position on the error of mode I stress intensity factor range; (b) Effect of forbidden zone size on the error of mode I stress intensity factor range.



The forbidden zone excludes the field data in the vicinity of the crack. To investigate sensitivity to the zone dimension, a group of forbidden zones with different lengths and widths was applied to a single dataset and the fluctuations in the range of stress intensity factor results were compared, as shown in Fig. 5(b). The dataset was for applied subset size of  $96 \times 96$  pixels, with an overlap of 75%, for an image dataset of  $800 \times 700$  pixels. The forbidden zone size was normalized in both directions of the dataset (X and Y) and medium size forbidden zone ( $0.75 \times 0.6$ ,  $240 \times 150$  pixels) was selected as reference to which the relative error of  $\Delta K_I$  was calculated. It can be seen that generally varying the dimension of the forbidden zone has a small effect on the  $\Delta K_I$  value, and the analysis approach for the elastic opening of the crack is robust to missing data in the vicinity of the crack.

#### 4. Conclusions

For the study of short fatigue cracks, the full-field DIC measurements have been used as boundary conditions for finite element calculation of the local J-integral and the stress intensity factors during the elastic monotonic opening of a fatigue crack. It has been demonstrated in a case study of short cracks in Zircoloy-4 that this method is insensitive to the specimen geometry and does not require any prior knowledge of the applied loading and the total crack length. Only the local crack tip segment is used within this framework, and it can be applied when DIC measurements in the vicinity of the crack surface are not trustworthy. Both Mode I and Mode II stress intensity factors can be extracted, which allows for a precise evaluation of the local crack tip conditions.

#### Acknowledgements

Abdalrhaman Koko is gratefully acknowledged for his assistance with finite element analysis.

#### References

- Anderson, T L. 2017. *Fracture Mechanics: Fundamentals and Applications, Fourth Edition*. CRC Press. Vol. 76.
- Barhli, S. M., M. Mostafavi, A. F. Cinar, D. Hollis, and T. J. Marrow. 2017. "J-Integral Calculation by Finite Element Processing of Measured Full-Field Surface Displacements." *Experimental Mechanics* 57 (6). <https://doi.org/10.1007/s11340-017-0275-1>.
- Becker, T. H., T. J. Marrow, and R. B. Tait. 2011. "Damage, Crack Growth and Fracture Characteristics of Nuclear Grade Graphite Using the Double Torsion Technique." *Journal of Nuclear Materials* 414 (1). <https://doi.org/10.1016/j.jnucmat.2011.04.058>.
- Becker, T. H., M. Mostafavi, R. B. Tait, and T. J. Marrow. 2012. "An Approach to Calculate the J-Integral by Digital Image Correlation Displacement Field Measurement." *Fatigue and Fracture of Engineering Materials and Structures* 35 (10). <https://doi.org/10.1111/j.1460-2695.2012.01685.x>.
- Bornert, M., F. Brémand, P. Doumalin, J. C. Dupré, M. Fazzini, M. Grédiac, F. Hild, et al. 2009. "Assessment of Digital Image Correlation Measurement Errors: Methodology and Results." *Experimental Mechanics* 49 (3). <https://doi.org/10.1007/s11340-008-9204-7>.
- Bruck, H. A., S. R. McNeill, M. A. Sutton, and W. H. Peters. 1989. "Digital Image Correlation Using Newton-Raphson Method of Partial Differential Correction." *Experimental Mechanics* 29 (3). <https://doi.org/10.1007/BF02321405>.
- Chen, D. J., F. P. Chiang, Y. S. Tan, and H. S. Don. 1993. "Digital Speckle-Displacement Measurement Using a Complex Spectrum Method." *Applied Optics* 32 (11). <https://doi.org/10.1364/ao.32.001839>.
- Christ, H. J., C. P. Fritzen, and P. Köster. 2014. "Micromechanical Modeling of Short Fatigue Cracks." *Current Opinion in Solid State and Materials Science*. <https://doi.org/10.1016/j.cossms.2014.05.001>.
- Duff, J. A., and T. J. Marrow. 2013. "In Situ Observation of Short Fatigue Crack Propagation in Oxygenated Water at Elevated Temperature and Pressure." *Corrosion Science* 68. <https://doi.org/10.1016/j.corsci.2012.10.030>.
- Hung, Po Chih, and A. S. Voloshin. 2003. "In-Plane Strain Measurement by Digital Image Correlation." *Journal of the Brazilian Society of Mechanical Sciences and Engineering* 25 (3). <https://doi.org/10.1590/S1678-58782003000300001>.
- King, A., W. Ludwig, M. Herbig, J. Y. Buffire, A. A. Khan, N. Stevens, and T. J. Marrow. 2011. "Three-Dimensional in Situ Observations of Short Fatigue Crack Growth in Magnesium." *Acta Materialia* 59 (17). <https://doi.org/10.1016/j.actamat.2011.07.034>.
- Koko, A., P. Earp, T. Wigger, J. Tong, and T. J. Marrow. 2020. "J-Integral Analysis: An EDXD and DIC Comparative Study for a Fatigue Crack." *International Journal of Fatigue* 134. <https://doi.org/10.1016/j.ijfatigue.2020.105474>.
- Limodin, Nathalie, Julien Réthoré, Jean Yves Buffière, Anthony Gravouil, François Hild, and Stéphane Roux. 2009. "Crack Closure and Stress Intensity Factor Measurements in Nodular Graphite Cast Iron Using Three-Dimensional Correlation of Laboratory X-Ray Microtomography Images." *Acta Materialia* 57 (14). <https://doi.org/10.1016/j.actamat.2009.05.005>.
- Liu, Jin, Jed Lyons, Michael Sutton, and Anthony Reynolds. 1998. "Experimental Characterization of Crack Tip Deformation Fields in Alloy 718 at High Temperatures." *Journal of Engineering Materials and Technology, Transactions of the ASME* 120 (1). <https://doi.org/10.1115/1.2806840>.
- Marrow, T. J., M. Mostafavi, T. Hashimoto, and G. E. Thompson. 2014. "A Quantitative Three-Dimensional in Situ Study of a Short Fatigue Crack

- in a Magnesium Alloy.” *International Journal of Fatigue* 66. <https://doi.org/10.1016/j.ijfatigue.2014.04.003>.
- McNeill, S. R., W. H. Peters, and M. A. Sutton. 1987. “Estimation of Stress Intensity Factor by Digital Image Correlation.” *Engineering Fracture Mechanics* 28 (1). [https://doi.org/10.1016/0013-7944\(87\)90124-X](https://doi.org/10.1016/0013-7944(87)90124-X).
- Moutou Pitti, Rostand, Claudiu Badulescu, and Michel Grédiac. 2014. “Characterization of a Cracked Specimen with Full-Field Measurements: Direct Determination of the Crack Tip and Energy Release Rate Calculation.” *International Journal of Fracture* 187 (1). <https://doi.org/10.1007/s10704-013-9921-5>.
- Newman, J. C., and I. S. Raju. 1986. “Stress-Intensity Factor Equations for Cracks in Three-Dimensional Finite Bodies Subjected to Tension and Bending Loads.” *Computational Methods in the Mechanics of Fracture* 2.
- Peters, W. H., and W. F. Ranson. 1982. “Digital Imaging Techniques In Experimental Stress Analysis.” *Optical Engineering* 21 (3). <https://doi.org/10.1117/12.7972925>.
- Réthoré, J., N. Limodin, J. Y. Buffière, F. Hild, W. Ludwig, and S. Roux. 2011. “Digital Volume Correlation Analyses of Synchrotron Tomographic Images.” *Journal of Strain Analysis for Engineering Design* 46 (7). <https://doi.org/10.1177/0309324711409999>.
- Réthoré, Julien, Nathalie Limodin, Jean Yves Buffière, Stéphane Roux, and Fran Çois Hild. 2012. “Three-Dimensional Analysis of Fatigue Crack Propagation Using X-Ray Tomography, Digital Volume Correlation and Extended Finite Element Simulations.” In *Procedia IUTAM*. Vol. 4. <https://doi.org/10.1016/j.piutam.2012.05.017>.
- Roux, S., J. Réthoré, and F. Hild. 2009. “Digital Image Correlation and Fracture: An Advanced Technique for Estimating Stress Intensity Factors of 2D and 3D Cracks.” *Journal of Physics D: Applied Physics* 42 (21). <https://doi.org/10.1088/0022-3727/42/21/214004>.
- Roux, Stéphane, and François Hild. 2006. “Stress Intensity Factor Measurements from Digital Image Correlation: Post-Processing and Integrated Approaches.” In *International Journal of Fracture*. Vol. 140. <https://doi.org/10.1007/s10704-006-6631-2>.
- Shih, C. F., and R. J. Asaro. 1989. “Elastic-Plastic Analysis of Cracks on Bimaterial Interfaces: Part II- Structure of Small-Scale Yielding Fields.” *Journal of Applied Mechanics, Transactions ASME* 56 (4). <https://doi.org/10.1115/1.3176170>.
- Vend Roux, G., and W. G. Knauss. 1998. “Submicron Deformation Field Measurements: Part 2. Improved Digital Image Correlation.” *Experimental Mechanics* 38 (2). <https://doi.org/10.1007/BF02321649>.
- Wan, Weifeng, and Fionn P.E. Dunne. 2020. “Microstructure-Interacting Short Crack Growth in Blocky Alpha Zircaloy-4.” *International Journal of Plasticity* 130. <https://doi.org/10.1016/j.iijplas.2020.102711>.
- Westerweel, Jerry, and Fulvio Scarano. 2005. “Universal Outlier Detection for PIV Data.” *Experiments in Fluids* 39 (6). <https://doi.org/10.1007/s00348-005-0016-6>.
- Wilkinson, Angus J. 2001. “Modelling the Effects of Texture on the Statistics of Stage I Fatigue Crack Growth.” *Philosophical Magazine A: Physics of Condensed Matter, Structure, Defects and Mechanical Properties* 81 (4). <https://doi.org/10.1080/01418610108214323>.
- Xu, Yilun, Weifeng Wan, and Fionn P.E. Dunne. 2021. “Microstructural Fracture Mechanics: Stored Energy Density at Fatigue Cracks.” *Journal of the Mechanics and Physics of Solids* 146. <https://doi.org/10.1016/j.jmps.2020.104209>.